Kinetic and Structural Analysis of Mutant *Escherichia coli* Dihydroorotases: A Flexible Loop Stabilizes the Transition State[†,‡]

Mihwa Lee,[§] Megan J. Maher,[||] Richard I. Christopherson,[§] and J. Mitchell Guss*[,§]

School of Molecular and Microbial Biosciences, University of Sydney, New South Wales 2006, Australia, and Division of Molecular Biosciences, Imperial College, London SW7 2ZA, U.K.

Received June 5, 2007; Revised Manuscript Received July 8, 2007

ABSTRACT: Dihydroorotase (DHOase) catalyzes the reversible cyclization of *N*-carbamyl-L-aspartate (CA-asp) to L-dihydroorotate (DHO) in the *de novo* biosynthesis of pyrimidine nucleotides. Two different conformations of the surface loop (residues 105−115) were found in the dimeric *Escherichia coli* DHOase crystallized in the presence of DHO (PDB code 1XGE). The loop asymmetry reflected that of the active site contents of the two subunits: the product, DHO, was bound in the active site of one subunit and the substrate, CA-asp, in the active site of the other. In the substrate- (CA-asp-) bound subunit, the surface loop reaches in toward the active site and makes hydrogen bonds with the bound CA-asp via two threonine residues (Thr109 and Thr110), whereas the loop forms part of the surface of the protein in the product- (DHO-) bound subunit. To investigate the relationship between the structural states of this loop and the catalytic mechanism of the enzyme, a series of mutant DHOases including deletion of the flexible loop were generated and characterized kinetically and structurally. Disruption of the hydrogen bonds between the surface loop and the substrate results in significant loss of catalytic activity. Furthermore, structures of these mutants with low catalytic activity have no interpretable electron density for parts of the flexible loop. The structure of the mutant (Δ107−116), in which the flexible loop is deleted, shows only small differences in positions of other substrate binding residues and in the binuclear zinc center compared with the native structure, yet the enzyme has negligible activity. The kinetic and structural analyses suggest that Thr109 and Thr110 in the flexible loop provide productive binding of substrate and stabilize the transition-state intermediate, thereby increasing catalytic activity.

Dihydroorotase (DHOase;[1] EC 3.5.2.3) catalyzes cyclization of *N*-carbamyl-L-aspartate (CA-asp) to L-dihydroorotate (DHO), the third step of the pathway for *de novo* biosynthesis of pyrimidine nucleotides (Scheme 1). The cyclization reaction is reversible and pH dependent (*1*, *2*). The biosynthetic direction, cyclization of CA-asp to DHO, is favored at lower pH, while the formation of CA-asp is dominant at alkaline pH. Using hamster DHOase, Christopherson and Jones found the equilibrium ratio of CA-asp/DHO to be unity at pH 6.2 (*1*).

As an integral part of the pyrimidine synthetic pathway, DHOase activity is important in providing pyrimidine nucleotides essential for cellular metabolism, serving as precursors for synthesis of DNA, RNA, phospholipids, UDP sugars, and glycogen (*3*). In higher eukaryotes, the activity of DHOase is contained in the trifunctional enzyme CAD that catalyzes the first three steps of the *de novo* pyrimidine synthesis including the activities of carbamyl phosphate synthetase (CPSase), aspartate transcarbamylase (ATCase), and DHOase (*4*). In bacteria and yeast, DHOase is monofunctional and usually homodimeric with a few monomeric exceptions (*5*−*7*).

A phylogenetic analysis of the amino acid sequences of DHOases groups them into two major classes that may have diverged from a common ancestor following gene duplication (*8*). Type I DHOases are more ancient and include the DHOase domain of mammalian CAD and monofunctional DHOases found in Gram-positive bacteria, including *Bacillus*, *Lactobacillus*, and *Streptococcus*. Type I DHOases can be divided further into three subgroups: type IA functions

[†] This work was supported by Grant DP0665282 from the Australian Research Council (J.M.G.). M.L. is supported by an Australian Postgraduate Award. Access to the Advanced Photon Source, Argonne National Laboratory, was made possible by a travel grant from the Access to Major National Facilities Program administrated by the Australian Nuclear Science and Technology Organization. GM/CA CAT has been funded in whole or in part with Federal funds from the National Cancer Institute (Y1-CO-1020) and the National Institute of General Medical Sciences (Y1-GM-1104). Use of the Advanced Photon Source was supported by the U.S. Department of Energy, Basic Energy Sciences, Office of Science, under Contract W-31-109-ENG-38.

[‡] The atomic coordinates and structure factor amplitudes have been deposited in the Protein Data Bank (www.rcsb.org) as entries 2Z24 (110 Ser mutant), 2Z25 (110 Val mutant), 2Z26 (110 Ala mutant), 2Z27 (109 Ser mutant), 2Z28 (109 Val mutant), 2Z29 (109 Ala mutant), 2Z2A (109 Gly mutant), and 2Z2B (107−116 deletion mutant).

* Address correspondence to this author: phone, +61 2 9351 4302; fax, +61 2 9351 4726; e-mail, m.guss@mmb.usyd.edu.au.

[§] University of Sydney.

[||] Imperial College.

[1] Abbreviations: ATCase, aspartate transcarbamylase; CA-asp, *N*-carbamylaspartate; CAD, carbamyl phosphate synthetase−aspartate transcarbamylase−dihydroorotase; CPSase, carbamyl phosphate synthetase; DHO, dihydroorotate; DHOase, dihydroorotase; DHU, dihydrouracil; DHPase, dihydropyrimidinase; FOA, 5-fluoroorotate; HEPES, *N*-(2-hydroxyethyl)piperazine-*N*′-2-ethanesulfonic acid; HDDP, 2-oxo-1,2,3,6-tetrahydropyrimidine-4,6-dicarboxylate; HYD, hydantoinase; MES, 2-morpholinoethanesulfonic acid; PTE, phosphotriesterase; URE, urease.

10.1021/bi701098e CCC: $37.00
Published on Web 08/21/2007

Scheme 1: Reversible Cyclization of CA-asp to DHO Catalyzed by DHOase

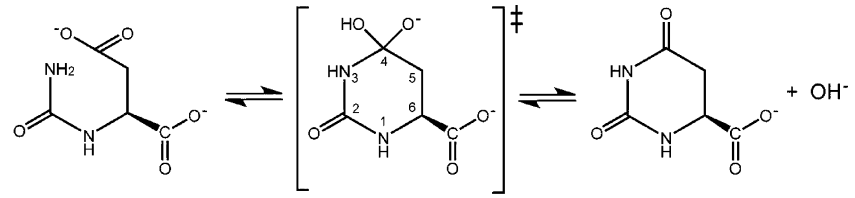

N-Carbamyl-L-aspartate (CA-asp) L-Dihydroorotate (DHO)

independently of any other enzyme in the pyrimidine pathway [e.g., DHOase from *Bacillus caldolyticus* (*9*, *10*)], type IB is fully functional only when interacting with one or more other enzymes of the pyrimidine pathway [e.g., DHOase from *Aquifex aeolicus* (*6*, *11*)], while type IC is covalently linked with at least one other enzyme in the pathway, exemplified by mammalian CAD. Type II DHOases are all monofunctional enzymes found predominantly in Gram-negative bacteria (e.g., *Escherichia coli*) and yeast. Type I enzymes have typical subunit molecular masses of ~45 kDa compared to ~38 kDa for the type II enzymes. Members of the same class of DHOase share relatively high identity in their amino acid sequences (>40%), but a low level of sequence identity (<~20%) is observed between the two classes.

DHOase belongs to the amidohydrolase superfamily that contains a variety of hydrolytic enzymes of the $(\beta/\alpha)_8$ barrel (or TIM-barrel) fold (*12*). The active sites of these enzymes have a mononuclear or binuclear metal center (Zn, Ni, or Fe), whose main role is to activate the scissile bond of the substrate for cleavage and to deprotonate a water molecule for nucleophilic attack (*13*). Virtually identical binuclear metal centers are found in *E. coli* DHOase (*14*, *15*), urease (URE) (*16*, *17*), phosphotriesterase (PTE) (*18*), hydantoinase (HYD) (*19*, *20*), and dihydropyrimidinase (DHPase) (*21*). The active sites are characterized by six highly conserved metal ligands including four histidine residues, one aspartate residue, and a carboxylated lysine, formed from the post-translational carboxylation of a lysine residue. The two divalent metal ions are bridged by a hydroxide ion in addition to the carbamate functional group derived from the modified lysine. Despite the strong similarity of the active sites between these enzymes, each enzyme catalyzes the hydrolysis of a different substrate.

DHOases from different sources have different metal contents that do not strictly correlate with the phylogenetic classification above. Although the *E. coli* DHOase, a type II DHOase, had been reported previously to have only one catalytic Zn per monomer (*22*−*24*), the structures [PDB codes 1J79 and 1XGE (*14*, *15*)] show that the active site contains a binuclear Zn center. A conserved lysine residue, presumably carboxylated to ligate two Zn atoms, is found in the sequence alignment of all known type II DHOases. Therefore, it is most likely that all type II DHOases contain two Zn atoms in the active site. In contrast, the metal content in type I DHOases still remains the subject of controversy. The first structures of a type I DHOase from *A. aeolicus* DHOase [1XRT/1XRF (*11*)] have only one Zn atom in the active site. The metal analysis study of the isolated CAD DHOase domain from hamster, a type I DHOase, also has only one Zn atom in the active site (*25*−*27*). Recently, another structure of a type I DHOase from *Porphyromonas gingivalis* (2GWN) has been deposited in the PDB by a structural genomics group without further publication. Interestingly, the structure of *P. gingivalis* DHOase has two Zn atoms, bridged by a carboxylated lysine, in the active site. Therefore, it is possible that certain groups of type I DHOases contain one Zn atom per active site whereas other groups contain two. The definite answer for the metal contents in DHOases will emerge when more structures of DHOases are solved, resulting in a revised classification of these enzymes.

The catalytic mechanism of DHOase has been probed by a number of methods including pH−rate profiles (*1*, *2*), site-directed mutagenesis (*2*, *28*, *29*), and the preparation of metal-substituted variants (*2*, *24*). Most recently, the crystal structures of *E. coli* DHOase have provided critical information on how the enzyme functions in atomic level detail (*14*, *15*). The structures of DHOase crystallized in the presence of D,L-CA-asp [PDB code 1J79 (*14*)] and L-DHO [PDB code 1XGE (*15*)], respectively, have unusual asymmetry in the active sites of the homodimeric enzyme: one subunit contains bound L-DHO and the other L-CA-asp. This unique situation allowed a detailed analysis of interactions of the enzyme with substrate and product. In addition, the structure crystallized in the presence of L-DHO shows that a surface loop, comprised of residues 105−115, adopts different conformations depending on whether substrate or product is present in the active site: In the substrate- (CA-asp-) bound subunit, this surface loop reaches in toward the active site and makes hydrogen bonds with the bound substrate via two threonine residues (Thr109 and Thr110) ("loop in"), whereas the loop forms part of the surface of the protein in the product- (DHO-) bound subunit ("loop out"). In a subsequent study, we reported structures of ligand-free and inhibitor complexes of *E. coli* DHOase and observed that the loop-in conformation can only be maintained when the substrate or the substrate-like molecule is present in the active site (*30*).

In this study, we have employed site-directed mutagenesis and X-ray crystallography to probe the role of the surface loop movement of *E. coli* DHOase in catalysis. We have generated a series of single-point mutants of Thr109 and Thr110 that interact with the bound substrate, CA-asp, in the active site of the wild-type enzyme. Thr109 interacts with one of the two carboxylate groups of CA-asp (Thr109 $O^{\gamma 1}\cdots$CA-asp O5, 2.6 Å) and Thr110 with the other carboxylate group (Thr110 $O^{\gamma 1}\cdots$CA-asp O62, 2.7 Å). These two threonine residues have been mutated to Ser, Val, Ala, or Gly. We have also generated two deletion mutants that lack the flexible loop. Examination of the wild-type structure showed that the $C^{\alpha}-C^{\alpha}$ distances between residues 106 and 116 and between residues 106 and 117 are about 5 Å (C^{α}-106−C^{α}116, 5.1 Å, and C^{α}106−C^{α}117, 5.0 Å, in the DHO-

bound subunit; $C^{\alpha}106-C^{\alpha}116$, 5.1 Å, and $C^{\alpha}106-C^{\alpha}117$, 5.6 Å, in the CA-asp-bound subunit). Since the normal $C^{\alpha}-C^{\alpha}$ distance in an extended amino acid chain is 3.8 Å, we reasoned that the intervening nine (or ten) residues could be excised and a new peptide bond could be introduced between residues 106 and 116 (or 117) without significantly distorting the overall protein structure. The nine (or ten) deleted residues include Thr109 and Thr110, and the resulting shortened loop should be unable to close the active site cavity during catalysis. Here we report analysis of catalytic activities and crystal structures of mutant DHOases. This defines the roles of the flexible loop in catalysis of *E. coli* DHOase, which provides a more complete catalytic mechanism for *E. coli* DHOase.

MATERIALS AND METHODS

Generation, Expression, and Purification of Mutant DHOases. E. coli strain X7014a, which lacks a gene for DHOase, was obtained from the Yale *E. coli* Genetic Stock Center (Yale University, New Haven, CT) and used for expression and purification of wild-type and mutant DHOases. Mutations in the gene for DHOase were generated using the QuikChange site-directed mutagenesis kit (Stratagene) and the mutagenic primers listed in Table 1 of the Supporting Information. The wild-type DHOase in the pBS+ vector was used as a template, and the mutations were confirmed by determination of the nucleotide sequences of the whole gene.

Purification procedures for wild-type DHOase and mutant enzymes were adapted from the previous report (*22*). Briefly, the soluble fraction of lysed cells in 20 mM HEPES (pH 7.2) containing 2 mM DTT was subjected to heat denaturation at 72 °C followed by centrifugation. The supernatant was fractionated using an ammonium sulfate cut from 45% to 60% saturation. The precipitate was redissolved and dialyzed against 20 mM HEPES (pH 7.2) buffer containing 1 mM DTT and applied to a MonoQ ion-exchange column (Pharmacia) and then eluted with a NaCl gradient (0.25−0.35 M). The final protein sample was dialyzed against the HEPES buffer and then concentrated using Microsep centrifugal devices with a molecular mass cutoff of 30 kDa (Pall). The purity of wild-type and mutant DHOases (>98% for all samples) was confirmed by SDS−PAGE.

Enzyme Kinetics. The DHOase activity was assayed spectrophotometrically at 230 nm (*31*). The linear increase in absorbance at 230 nm due to formation of DHO (ϵ_{230} = 1.17 mM^{-1} cm^{-1}) was measured, and initial reaction rates were calculated. The enzyme assays were performed in 96-well plates (Costar UV-plate; Corning). Reaction mixtures contained 0.1 M potassium phosphate (pH 5.8) and substrate, D,L-CA-asp (Sigma), in the range of 0.25−20 mM in a total volume of 250 μL and were preincubated at 30 °C prior to the assay. Reactions were initiated by addition of purified enzyme to the assay mixture using a Mosquito nanoliter liquid handling robot (TTP LabTech). The typical volume of added enzyme in the reaction was in the range of 0.4−0.8 μL. Kinetic parameters (K_s and k_{cat}) were obtained by fitting experimental data to the Michaelis−Menten equation by nonlinear regression using the program PRISM 4 (GraphPad Software).

Protein Crystallization and X-ray Diffraction. Crystals of mutant DHOase were grown by the hanging-drop vapor diffusion method using conditions similar to those reported previously (*15*). A drop containing 2 μL of protein solution (6−8 mg mL^{-1}) was mixed with 2 μL of reservoir solution (15−20% polyethylene glycol 3350, 0.1 M MES, pH 6.0−6.5, 75 mM $MgCl_2$, and 150 mM KCl) and 0.45 μL of 100 mM L-DHO, giving a final ligand concentration of 10 mM. Diffraction-quality crystals were harvested after 4 days of equilibration against reservoir solution at 277 K for all single-point mutants and after 2 weeks for the deletion mutant (Δ107−116).

Prior to data collection, the crystals were transferred to cryoprotectant solution consisting of the mother liquor solution containing 18% glycerol and then flash-cooled in a stream of nitrogen gas at 100 K. Laboratory diffraction data were recorded at 100 K on a Mar345 imaging plate detector (Marresearch) using X-rays produced by a Rigaku RU200H rotating anode generator (Cu K_{α}, λ = 1.5418 Å), focused with Osmic mirrors (MSC Rigaku). The diffraction data were processed and scaled with the *HKL* suite of programs, DENZO and SCALEPACK (*32*). Synchrotron diffraction data were recorded on beamline 23-ID at the Advanced Photon Source, Argonne National Laboratory, using a CCD detector, MARmosaic 300 (Marresearch), with the wavelength of 0.9793 Å at 100 K. The synchrotron diffraction data were processed and scaled with HKL2000 (*32*). Crystals of the single-point mutants were isomorphous with the previously reported structure of the wild-type DHOase [PDB code 1XGE (*15*)]. The deletion mutant (Δ107−116) was indexed in space group *P*312 with unit cell dimensions $a = b$ = 52.3 Å and c = 216.0 Å. The Matthew's coefficient (*33*) for space group *P*312 (V_M = 2.3 $Å^3$ Da^{-1}) suggests there is one monomer per asymmetric unit giving a calculated solvent content of 46.2%. Statistics for the data collection are presented in Table 1.

Structure Solution and Refinement for Single-Point Mutants. The structure of the wild-type DHOase solved previously in the same space group [PDB code 1XGE (*15*)] was used as the initial model for the refinement of the structures of the single-point mutants. All nonprotein atoms [metals, ligands (L-DHO and L-CA-asp), and solvent atoms] were removed from the initial model. Residues B106−114 were also deleted to avoid model bias. The initial model was refined initially as a rigid body using diffraction data to 3.0 Å resolution with REFMAC5 (*34*).

Subsequent refinement was carried out using all available diffraction data in rounds, which included iterative cycles of TLS (*35*) and restrained refinement in REFMAC5 (*34*) with manual model building using the program COOT (*36*). The positions of the two Zn atoms at each active site were identified in the early stage of refinement from the calculated difference Fourier electron density maps and were included in the model. The addition of solvent molecules was carried out using ARP/wARP (*37*) in conjunction with manual inspection of electron density maps in COOT with consideration of hydrogen-bonding criteria. Residues B106−114 were built into residual positive difference electron density in the T110V mutant structure after completion of solvent building. Finally, positive electron density in difference Fourier maps within the active site cavities of each subunit was modeled with the respective ligands (L-DHO or L-CA-asp).

Structure Solution and Refinement for the Deletion Mutant. The structure of the deletion mutant (Δ107−116) was solved

Table 1: Data Collection and Refinement Statistics

	crystal							
	T110S DHOase	T110V DHOase	T110A DHOase	T109S DHOase	T109V DHOase	T109A DHOase	T109G DHOase	Δ107−116 DHOase
Crystal and Diffraction Data								
X-ray source	rotating anode	rotating anode	APS 23-ID	rotating anode	rotating anode	rotating anode	rotating anode	APS 23-ID
λ (Å)	1.5418	1.5418	0.9793	1.5418	1.5418	1.5418	1.5418	0.9793
space group	$P2_12_12_1$	$P2_12_12_1$	$P2_12_12_1$	$P2_12_12_1$	$P2_12_12_1$	$P2_12_12_1$	$P2_12_12_1$	$P3_212$
unit cell dimensions								
a (Å)	51.4	51.4	51.5	51.4	51.4	51.3	51.4	52.3
b (Å)	78.8	79.0	78.9	78.5	78.4	78.5	78.2	52.3
c (Å)	180.2	180.5	180.1	180.2	180.0	180.5	180.0	216.0
resolution range (Å)[a]	40−1.90 (1.95−1.90)	40−1.87 (1.92−1.87)	32−1.29 (1.32−1.29)	40−1.87 (1.92−1.87)	40−1.87 (1.92−1.87)	40−1.90 (1.95−1.90)	40−1.87 (1.92−1.87)	40−1.85 (1.90−1.85)
unique reflections	56580	60822	166743	59086	58553	56793	56036	28254
completeness (%)[a]	96.6 (95.7)	98.4 (96.2)	91.1 (49.8)	96.5 (89.1)	95.9 (97.8)	97.2 (94.3)	91.9 (91.7)	95.9 (92.5)
redundancy[a]	3.5 (2.3)	3.6 (2.3)	6.8 (3.1)	4.5 (3.5)	4.6 (2.8)	4.7 (3.5)	4.6 (3.9)	8.2 (6.0)
average $I/\sigma(I)$[a]	18.1 (3.1)	24.3 (4.2)	20.5 (3.0)	30.4 (8.7)	22.7 (6.4)	18.0 (4.5)	34.1 (8.7)	17.4 (2.6)
R_{merge}[a,b]	0.077 (0.311)	0.048 (0.219)	0.071 (0.363)	0.041 (0.141)	0.064 (0.189)	0.051 (0.283)	0.048 (0.152)	0.077 (0.630)
Wilson *B* value (Å)	25.5	24.2	16.1	24.8	25.5	26.4	25.2	40.6
Refinement Statistics								
R_{cryst}[a,c]	0.149 (0.199)	0.147 (0.176)	0.129 (0.156)	0.146 (0.166)	0.154 (0.167)	0.147 (0.177)	0.152 (0.162)	0.191 (0.247)
R_{free}[a,d]	0.198 (0.275)	0.185 (0.248)	0.154 (0.200)	0.188 (0.237)	0.189 (0.216)	0.188 (0.234)	0.196 (0.244)	0.245 (0.316)
protein atoms including Zn atoms	5339	5384	5371	5357	5322	5360	5318	2558
water atoms	572	668	782	590	506	505	583	136
ligand atoms[e]	23	23	34	23	23	23	34	
mean protein *B* factor (Å^2)								
subunit A	31.4	29.0	19.0	29.7	30.3	30.0	32.6	57.4
subunit B	32.1	29.7	22.0	30.6	32.1	29.7	33.0	
mean ligand *B* factor (Å^2)								
subunit A	28.0	27.2	16.4	27.0	26.9	30.9	27.7	
ubunit B	34.2	26.7	16.7	29.2	30.6	32.8	29.0	
rmsd bond lengths (Å)[f]	0.01	0.01	0.01	0.01	0.01	0.01	0.01	0.01
rmsd bond angles (deg)[f]	1.47	1.27	1.36	1.37	1.40	1.39	1.44	1.51
ESU (Å)[g]	0.09	0.08	0.02	0.07	0.07	0.08	0.08	0.11
PDB code	2Z24	2Z25	2Z26	2Z27	2Z28	2Z29	2Z2A	2Z2B

[a] The values in parentheses are for the highest resolution shell. [b] $R_{merge} = \sum_h\sum_i|I_{hi} - \langle I_h\rangle|/\sum_h\sum_i\langle I_h\rangle$. [c] $R_{cryst} = \sum_h|F_h(\text{obs}) - F_h(\text{calc})|/\sum_h F_h(\text{obs})$. [d] Approximately 5% of the reflections were reserved for the calculation of R_{free}. [e] CA-asp and/or DHO in the active sites of each structure. [f] Diffraction-component precision index (*50*) calculated using REFMAC (*34*). [g] Estimated standard uncertainty in atomic position, based on maximum likelihood (*34*, *50*).

by molecular replacement using PHASER from the CCP4 suite (*38*, *39*). Chain A of the wild-type DHOase structure [PDB code 1XGE (*15*)] was used as the search model. The Zn atoms, ligand molecule, solvent molecules, and residues 106−117 were deleted from the search model.

The fast rotation function of PHASER found one significant solution, which was then used for fast translation searches in all three possible space groups *P*312, $P3_112$, and $P3_212$. The best solution was found in $P3_212$; the *Z* score and the log-likelihood gain (LLG) increased from 20.7 to 33.4 and from 247 to 1520, respectively, after the fast translation function. The same refinement protocol used for the structures of single-point mutants was applied to the structure of the deletion mutant (Δ107−116).

Analysis and validation of all structures were carried out with the assistance of the program WHATCHECK (*40*) and the MOLPROBITY server (*41*). The refinement statistics are included in Table 1.

RESULTS

Mutations Decrease Catalytic Efficiency. The effects of mutations on the steady-state parameters k_{cat}, K_s, and k_{cat}/K_s were determined in the biosynthetic direction (CA-asp → DHO) at pH 5.8 (Table 2). The deletion mutants have negligible activities. Mutations at Thr110 also caused significant decreases in the catalytic activities, which nevertheless remained significant and measurable. Mutation to Ala (T110A) caused the most significant decrease in k_{cat}/K_s (43-fold) among the Thr110 mutants, indicating the importance of the hydrogen bond between the carboxylate group of CA-asp and $O^{\gamma 1}$ of Thr110. Despite the conservative nature of the mutation, Ser for Thr, this mutant has a substantially lower catalytic efficiency with a 6-fold decrease in k_{cat}/K_s. Interestingly, despite being unable to form the proposed hydrogen bond to CA-asp, the T110V mutant exhibits a slightly higher catalytic efficiency (2.4×10^4 M^{-1} s^{-1}) than the T110S mutant (2.0×10^4 M^{-1} s^{-1}). The T110V

Table 2: Kinetic Parameters of Mutant DHOases[a]

	k_{cat} (s^{-1})	K_s (mM)	k_{cat}/K_s ($M^{-1}\,s^{-1}$)	fold decrease k_{cat}/K_s
wild type	181.1 ± 3.3	1.5 ± 0.1	1.2×10^5	
T109S	49.8 ± 2.0	6.0 ± 0.7	8.3×10^3	15.1
T109V	<0.1	nd[b]	nd[b]	
T109A	<0.1	nd[b]	nd[b]	
T109G	<0.1	nd[b]	nd[b]	
T110S	59.7 ± 2.0	3.0 ± 0.3	2.0×10^4	6.3
T110V	145.5 ± 6.4	6.0 ± 0.7	2.4×10^4	5.1
T110A	11.5 ± 0.5	4.0 ± 0.6	2.9×10^3	43.4
Δ107−115	<0.1	nd[b]	nd[b]	
Δ107−116	<0.1	nd[b]	nd[b]	

[a] Mean of three independent measurements (±SEM) for the cyclization of CA-asp to DHO at pH 5.8. [b] Activity below the detection limit of the assay.

mutant has a higher K_s value (6.0 mM) compared to the wild-type (1.5 mM) or the T110S (3.0 mM) enzymes, but the k_{cat} value (145.5 s^{-1}) is higher than that of T110S (59.7 s^{-1}).

Of the four Thr109 mutants, only T109S has significant catalytic activity with k_{cat} of 49.8 s^{-1} and K_s of 6.0 mM (Table 2). In contrast to the mutations at residue Thr110, the substitution of Thr109 with Val, Ala, or Gly resulted in negligible catalytic activity.

Mutations Cause Transition of Crystal Forms. To elucidate the effects of mutations on the loop movement in relation to the catalytic activity, we crystallized the mutant enzymes in the presence of L-DHO. Most single-point mutants first grew in a tetragonal crystal form in the presence of L-DHO. These crystals were very unstable and disintegrated shortly after formation. Wild-type-like orthorhombic crystals then grew from the remnants of the tetragonal crystals or at new nucleation sites in the same drops. A structure of the tetragonal crystal form was solved eventually by stabilizing the crystals in the presence of a product-like inhibitor, 5-fluoroorotate (FOA) in place of L-DHO (*42*). Interestingly, in this structure, the flexible loops are both in the loop-out conformation, consistent with FOA, a product-like inhibitor, binding at both sites. The transition from one crystal form (tetragonal) to the other (orthorhombic) in the presence of DHO may be explained by presuming that DHO initially binds to both subunits with the loops in the "out" conformation, followed by slow conversion to CA-asp in the mutant enzymes with consequent movement of the flexible loop and dissolution of the crystals. Orthorhombic crystals isomorphous to the wild type are then able to grow in the presence of DHO and CA-asp with one loop out and the other in. The transition between crystal forms we observed with mutant enzymes provides further evidence that the loop movement is connected with the catalytic state of the enzyme.

Molecular Structures of Single-Point Mutants. The structures of seven single-point mutants of *E. coli* DHOase are reported with relatively high resolutions, ranging from 1.90 to 1.29 Å (Table. 1). The presence of the expected mutation was confirmed in all structures during the early stages of refinement. The overall structure of DHOase is not significantly affected by the mutations. The root mean squared deviations (rmsd) between the common C^α atoms in wild-type [PDB code 1XGE (*15*)] and mutant enzymes vary from 0.15 to 0.28 Å, consistent with expected errors in the coordinates. Structural differences between the wild type and mutants were generally small and restricted to the close vicinity of the flexible loop of subunit B.

All crystals of single-point mutants reported here are isomorphous with the wild-type crystal reported previously [PDB code 1XGE (*15*)], with a dimer in the asymmetric unit. The active site in subunit A of each structure contains L-DHO with the corresponding flexible loop in the out conformation. The packing of molecules in this particular crystal form preferentially stabilizes a loop-out conformation for subunit A through several hydrogen-bonding interactions with a neighboring symmetry-related molecule ($-x + 1$, $y + {}^1/_2$, $-z + {}^1/_2$). The loop-out conformation for subunit B, however, is precluded by unfavorable steric clashes with neighboring symmetry-related molecules. Interestingly, of the seven structures of single-point mutant enzymes, only T110V that has the highest turnover number among the mutant enzymes displays defined density for the flexible loop of subunit B (Figure 1a). The identity of the bound ligand in the active site of subunit B is clearly L-CA-asp as observed in subunit B of the wild-type structure. The loop in subunit B adopts the "in" conformation and interacts with the bound L-CA-asp in the active site as observed in the wild-type structure [PDB code 1XGE (*15*)]. Thr109 maintains the interaction with CA-asp (T109 $O^{\gamma 1}$···CA-asp O5, 2.6 Å), but the mutation of Thr110 to Val ($O^{\gamma 1}$ to $C^{\gamma 2}$) disrupts the hydrogen-bonding interaction observed in the wild-type structure. The resulting distance between O62 of CA-asp and $C^{\gamma 2}$ of Val110 is 3.3 Å. Other mutant enzymes that have measurable activity (T110S, T110A, and T109S) as well as those with very low activity (T109V, T109A, and T109G) show no interpretable electron density for parts of the flexible loop in subunit B. Specifically, residues B108−114 for T110S, residues B107−114 for T110A and T109V, residues B108−113 for T109S and T109A, and residues B106−116 for T109G are omitted from the models.

The bound ligand in the active site of subunit B of T110S, T109S, T109V, and T109A is modeled as CA-asp, although residual positive density that corresponds to the bond N3−C4 of DHO was detected in the $F_o - F_c$ map in the final stage of refinement. The residual density was very weak and not convincing enough to model L-DHO with partial occupancy. Nevertheless, it suggests that DHO was not fully converted to CA-asp in subunit B of these mutant enzymes. The corresponding flexible loops in subunit B are disordered. However, the C^α positions of the terminal residues of the disordered loop superpose well with the loop-in conformation of the wild-type enzyme.

In the cases of T109G and T110A, residual electron density in subunit B clearly indicates that a mixture of CA-asp and DHO is present in the active site. The final models for these two mutant enzymes include CA-asp and DHO in the active site of subunit B with half-occupancy each. However, the corresponding flexible loops in subunit B of these mutant enzymes are disordered. In these two mutants, the C^α positions of the terminal residues of the disordered loops are significantly different from the loop-in conformation observed in the wild-type enzyme (Figure 1b). In particular, in T109G, the terminal residues of the flexible loop are closer to the same residues of the loop-out conformation than to those of the loop-in conformation. This displacement in turn changes the positions of residues in the nearby loop (residues 80−85). The specific interactions

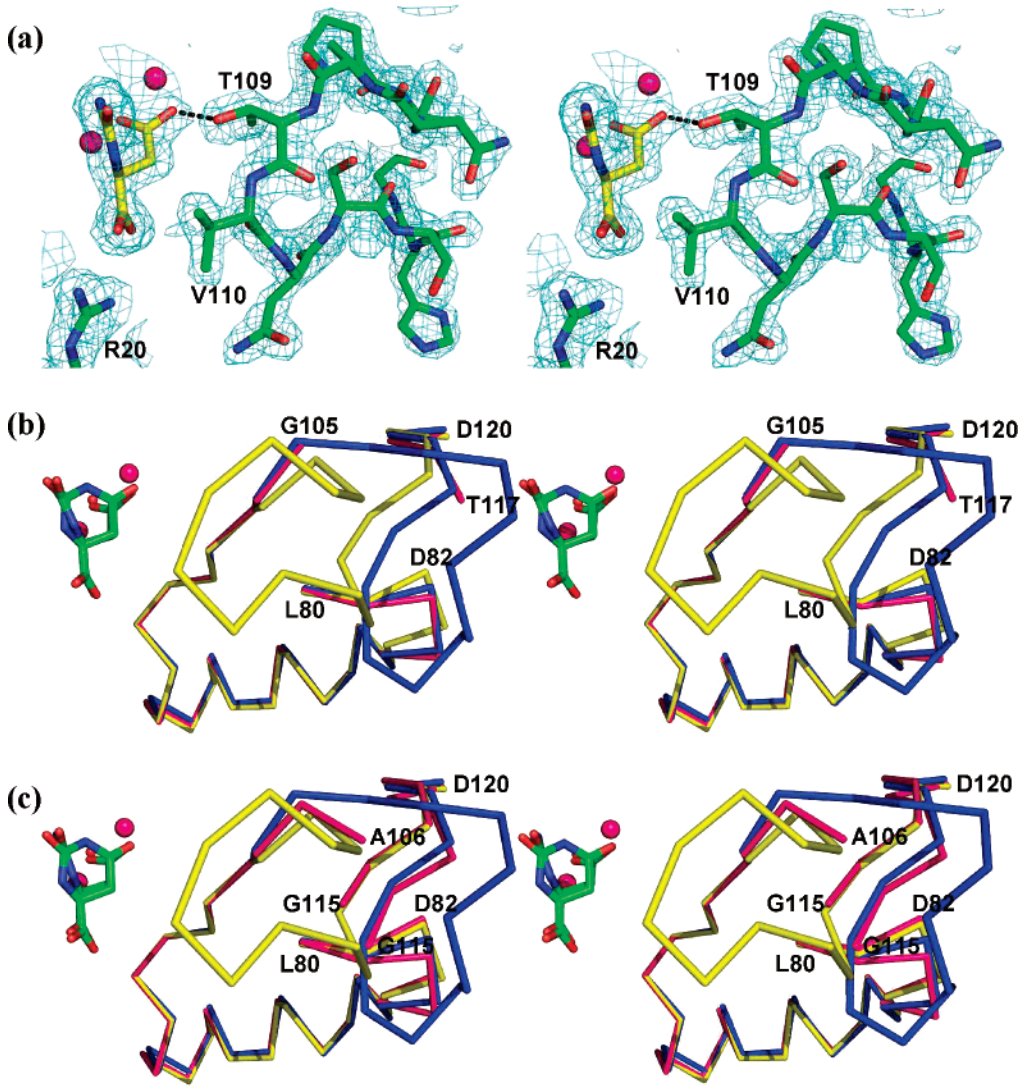

FIGURE 1: (a) Electron density map corresponding to the flexible loop (residues 105−115) in subunit B of the structure of the T110V mutant. The $2F_o - F_c$ map is contoured at 1.0σ. CA-asp, bound at the active site of subunit B of T110V, is shown with its carbon atoms colored yellow. A hydrogen bond between Thr109 and the bound CA-asp is indicated as a dashed line. The Zn atoms are shown as magenta spheres. (b, c) T109G (b) and T110A (c) mutants. C^{α} traces of residues 80−120 of each structure superposed with subunits A and B of the wild-type structure [PDB code 1XGE (*15*)] are shown in magenta, blue, and yellow, respectively. PyMOL was used to prepare the molecular images (*49*).

between the flexible loop and the adjacent loop (residues 80−85) are mediated by hydrogen bonds between residues Thr117 and Asp82 (Thr117 $O^{\gamma 1}$···Asp82 $O^{\delta 2}$ and Thr117 N···Asp82 $O^{\delta 1}$). The resulting positions of the adjacent loop (residues 80−85) are similar to those found in subunit A. Overall, the termini of the disordered flexible loop in subunit B of T109G take on the conformation that is similar to the loop-out conformation found in subunit A.

The structure of T110A refined with the highest resolution data (1.29 Å) shows heterogeneity of the C^{α} positions of the terminal residues of the flexible loop in subunit B. In this case, two alternate conformations of residues 115−120 are modeled: one similar to the loop-in conformation and the other to the loop-out conformation (Figure 1c). The heterogeneity affects the position of the adjacent loop comprised of residues 80−85 and results in two alternate conformations of residues 81−84.

Molecular Structures of the Deletion Mutant (Δ107−116). Crystals of the Δ107−116 mutant are hexagonal, space group $P3_212$, with unit cell dimensions $a = b = 52.3$ Å and $c = 216.0$ Å. The asymmetric unit contains only one monomer. Therefore, the biological dimer in the crystal is composed of two identical monomers. The structure was refined to 1.85 Å resolution with residuals of $R = 0.191$ and $R_{free} = 0.245$. The final model contains 331 amino acids (residues 6−336), 136 water molecules, and two Zn atoms. The overall structure of the Δ107−116 mutant is not significantly different from that of the wild-type DHOase except for the deleted peptide. When the structure of the Δ107−116 mutant is superposed on the structure of the wild-type DHOase [PDB code 1XGE (*15*)], the rmsd for 331 common C^{α} positions in each subunit are 0.55 and 0.52 Å, respectively. Structural differences are mainly concentrated close to the vicinity of the newly formed peptide bond (Figure 2a). Deletion of residues 107−116 and introduction of a new peptide bond between residues 106 and 117 significantly displace residues 106, 117 (107 for the mutant), and 118 (108 for the mutant). The differences in the C^{α} positions of these residues are 3.7, 4.5, and 2.0 Å, respectively, when subunit A of the wild-type structure is superposed onto the deletion mutant. The C^{α} atoms of

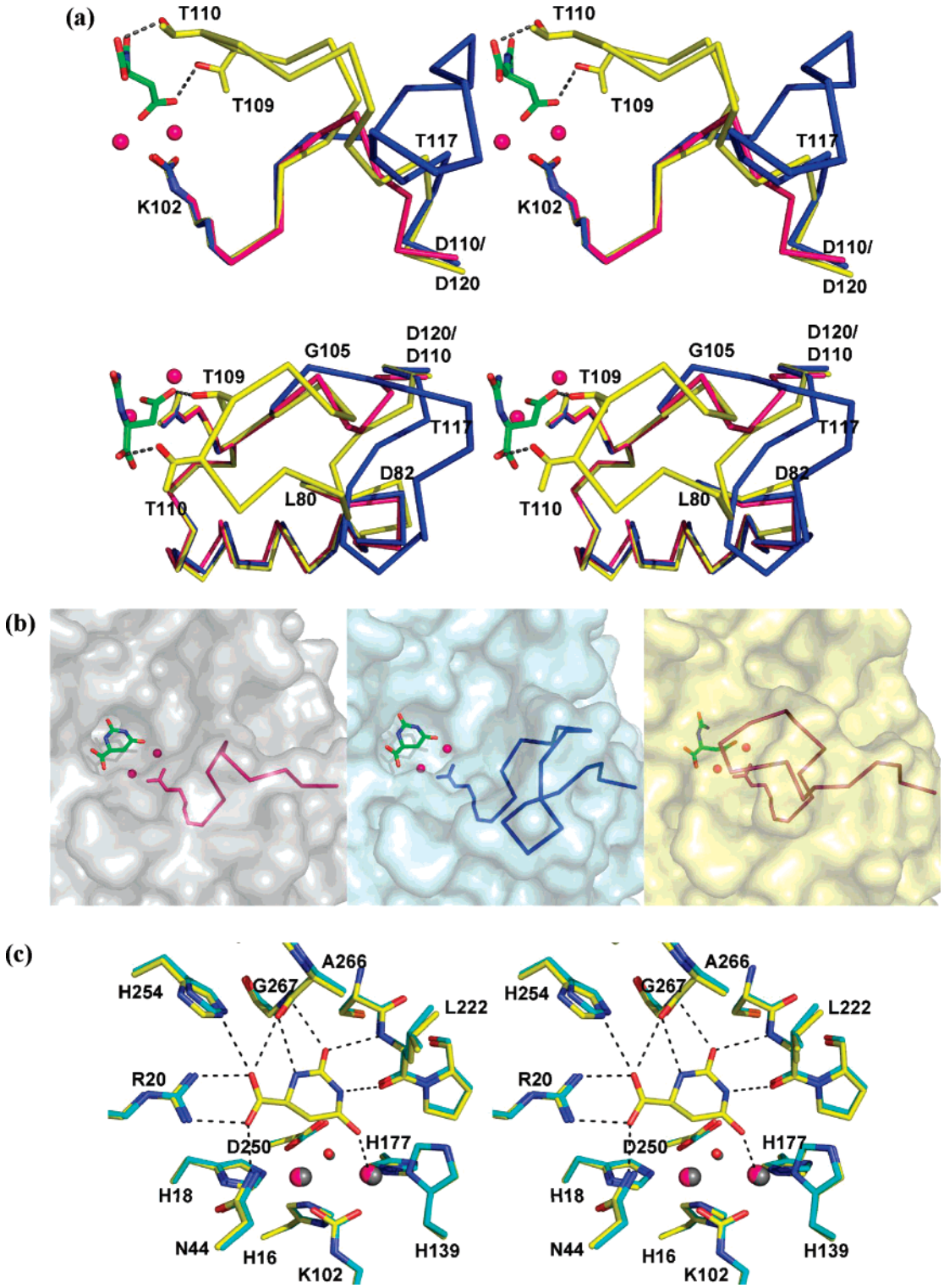

FIGURE 2: Structure of the deletion mutant (Δ107−116). (a) Superposition of the flexible loops. The Zn atoms are shown as magenta spheres. C^{α} traces of residues 102−120 of subunits A and B of the wild-type structure [PDB code 1XGE (*15*)] and residues 102−110 for the Δ107−116 mutant are shown in blue, yellow, and magenta, respectively. CA-asp, bound at the active site of subunit B of the wild-type structure, is shown for reference with its carbon atoms colored green. Hydrogen bonds to the bound CA-asp are depicted as dashed lines. (b) Surface representations of the Δ107−116 mutant (gray) and subunits A (pale cyan) and B (pale yellow) of the wild-type structure with the bound ligand in the active site. The DHO molecule drawn in the active site of the Δ107−116 mutant is indicated for reference only. C^{α} traces of residues 102−120 (residues 102−110 for the Δ107−116 mutant) are shown. (c) Superposition of the active sites of the Δ107−116 mutant and the wild-type enzyme with bound DHO. The structure of subunit A of the wild-type enzyme is shown as sticks with C^{α} atoms in yellow. The Zn atoms and the bridging water molecule for the wild-type enzyme are shown as magenta and red spheres, respectively. The C^{α} atoms of the Δ107−116 mutant are colored in cyan. The Zn atoms and the bridging water molecule for the Δ107−116 mutant are presented as gray spheres. Hydrogen bonds to the bound DHO in the wild-type enzyme are depicted as dashed lines.

residues 106 and 107 of the deletion mutant lie in approximately the same positions as those of residues B106 and B116 of the wild-type structure. Deletion of these residues results in the loss of the hydrogen bonds between

the flexible loop and the adjacent loop (residues 80−85) that involve residues Thr117 and Asp82. The resulting position of the 80−85 loop is similar to that observed in subunit A of the wild-type structure (Figure 2a).

Surface representations of the Δ107−116 mutant and the two subunits of the wild-type structure show that the active site cavity of the Δ107−116 mutant is indeed similar to that of subunit A with the loop-out conformation (Figure 2b). Removal of the portion of the flexible loop that interacts with the substrate caused little effect on other substrate-binding residues in the active site cavity. When the Δ107−116 mutant and subunit A (DHO-bound) of the wild-type structure are superposed, no significant differences in other substrate binding residues are observed (Figure 2c). In the wild-type structure crystallized with DHO (PDB code 1XGE), the product molecule (DHO) is held in place by four side-chain atoms (Arg20 $N^{\eta 1}$ and $N^{\eta 2}$, Asn44 $N^{\delta 2}$, and His254 $N^{\epsilon 2}$) and three main-chain atoms (Leu222 N and O and Ala266 O) of subunit A. The substrate- (CA-asp-) bound subunit coordinates the substrate molecule using some of the same atoms (Arg20 $N^{\eta 1}$ and $N^{\eta 2}$, Asn44 $N^{\delta 2}$, Leu222 N and O, and Ala266 O) with the addition of Thr109 $O^{\gamma 1}$ and Thr110 $O^{\gamma 1}$ from the flexible loop. In the structure of the Δ107−116 mutant, four side-chain atoms provided by Arg20, Asn44, and His254 and the main-chain atoms of Leu222 and Ala266 are found in approximately the same positions as those of the wild-type structure. Interestingly, no electron density for DHO was found in the active site of the mutant despite the presence of the substrate binding residues and an excess of DHO in the crystallization medium.

DISCUSSION

Conformational changes during catalysis have been observed in many different enzymes and appear to be a general feature of many enzyme mechanisms (*43*−*45*). Although, in most enzymes, the optimization of the structures for each step in the reaction sequence seems to be achieved by subtle cooperative conformational changes (*45*, *46*), some enzymes undergo significant structural changes during substrate binding, conversion of substrate to product, and product release. These changes, particularly those associated with surface loops, are thought to fulfill a number of roles in catalysis: enhanced binding of substrate, correct orientation of catalytic groups, removal of water from the active site, and protection of intermediates from solvent.

Following the structure of *E. coli* DHOase crystallized in the presence of L-DHO (*15*), we reported the structures of the ligand-free and inhibitor complexes of *E. coli* DHOase (*30*). The ligand-free structure of *E. coli* DHOase showed little difference in the active site architecture in comparison to that of the ligand-bound structures. The residues involved in substrate or product binding reside in approximately the same positions as in the ligand-free structure. However, we observed a significant difference in the conformation of the flexible loop (residues 105−115). In the absence of a moiety that can stabilize the loop-in conformation, the loop was disordered as shown in the structures of the ligand-free and the DHOase−FOA complex (a product-like inhibitor). In contrast, the structure of DHOase complexed with HDDP, an inhibitor that has features of both the substrate and product, showed ordered density for the loop-in conformation. These observations reinforced the theory that the loop-in conformation can only be maintained by occupancy of a ligand (substrate or substrate analogue) that makes proper interactions with the loop.

The kinetic and structural analyses of mutant DHOases reported here provide further support for the importance of the flexible loop in catalysis by *E. coli* DHOase. Mutations in two threonine residues that make direct interactions with the bound substrate caused significant loss of catalytic activity. Specifically, mutants of Thr109 have activities as low as those of the deletion mutants, indicating the essential nature of this residue.

Roles of Residues Thr109 and Thr110 in Catalysis. In the wild-type structure crystallized in the presence of L-DHO, the exocyclic carboxylate group (C61, O61, and O62) of CA-asp interacts with Thr110 and is held by contacts with the side chains of Arg20 and Asn44. In the DHO-bound subunit, when the loop is in the out conformation, the interaction contributed by Thr110 $O^{\gamma 1}$ to CA-asp O62 is replaced by His254 $N^{\epsilon 2}$ (Schemes 1 and 2). In contrast, $O^{\gamma 1}$ of Thr109 interacts with the other carboxylate group (C4, O4, and O5) of CA-asp that is converted to a carbonyl group of DHO.

Mutations of Thr110 resulted in decreased but measurable activities (Table 2). The decreased activity of the conservative Thr to Ser mutation presumably results from the greater conformational flexibility of the Ser side chain, which destabilizes the interaction with the substrate. Replacement of Thr110 with Val has a larger effect on the K_s value than on k_{cat}, resulting in the highest k_{cat} and K_s values among the Thr110 mutants. Therefore, the effect on catalytic efficiency results mainly from an increase in K_s, supporting a role for this side chain in substrate binding. The results further suggest that although the hydrogen-bonding interaction with the substrate is lost in the Thr to Val mutant, the catalytic rate is maintained close to the wild-type value, indicating that the substrate is bound in a productive conformation. In contrast, T110S that can still provide the hydrogen-bonding interaction may not maintain the stable configuration required for positioning of the substrate due to the greater conformational flexibility of the Ser side chain. The kinetic data also agree with the crystallographic observation that T110V is the only mutant enzyme that has an ordered conformation of the flexible loop in subunit B with CA-asp bound. The corresponding loops in other mutant structures are disordered presumably because of the reduced affinity with the substrate and/or the presence of uncatalyzed DHO in the active site of subunit B.

With the exception of T109S, mutations at residue Thr109 result in negligible DHOase activity, indicating that the hydroxyl group of the side chain is essential for catalysis. Unlike the observations made in T110V, the hydrogen-bonding interaction between Thr109 and the substrate is essential for the conversion of CA-asp to DHO. Thr109 specifically interacts with the carboxylate group (C4, O4, and O5) of CA-asp that is converted to the carbonyl group of DHO via a tetrahedral transition-state intermediate (Schemes 1 and 2). The results suggest that the side chain of Thr109 contributes significantly to catalytic efficiency by enhancing substrate affinity and/or stabilizing the transition state.

Analysis of the structure of the deletion mutant, Δ107−116, reveals that there are no significant differences in the

Scheme 2: Proposed Catalytic Mechanism for *E. coli* DHOase

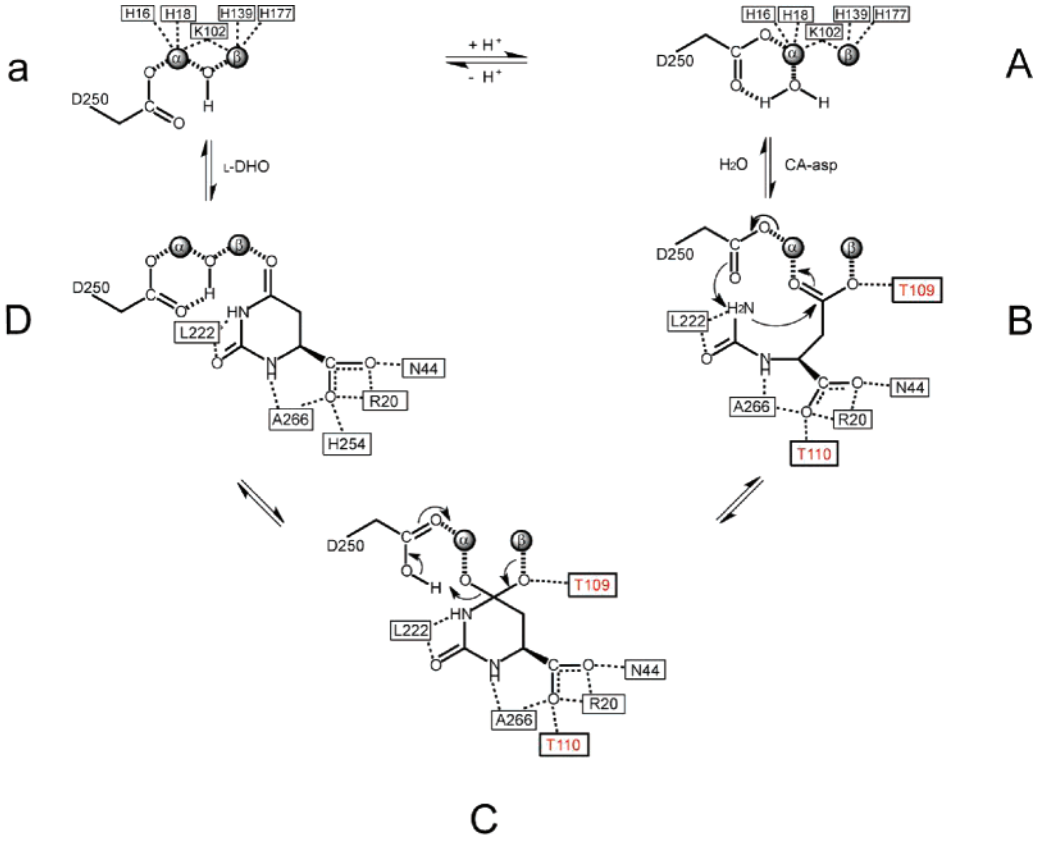

positions of other substrate binding residues and in the binuclear Zn center. Despite this, the mutant enzyme has negligible catalytic activity. Furthermore, there is no significant electron density for DHO in the active site despite the presence of excess DHO in the crystallization medium. This suggests that although the flexible loop is not required directly in binding DHO in the loop-out conformation, the dynamics of the loop movement are likely to be involved indirectly in the binding of DHO. It is, however, not clear how this process is achieved on the basis of current data. Overall, the data presented here support the proposal that the flexible loop contributes to positioning the substrate in the correct configuration for catalysis and also to increasing the affinity for the substrate- and/or transition-state intermediate.

Enzyme Mechanism. Reaction mechanisms for *E. coli* DHOase have been proposed previously on the basis of the crystallographic study (*14*), pH−rate profile, mutagenesis, and solvent isotope effects (*2*). However, these mechanisms were proposed before observation of the loop movement in *E. coli* DHOase was made and therefore do not account for the possible importance of the loop movement. The observation of the two conformations of the flexible loop provides a more complete picture of the catalytic mechanism of *E. coli* DHOase (Scheme 2). When there is no substrate in the active site, the flexible loops in each subunit can move in and out dynamically. When substrate (CA-asp) enters the active site, it induces closure of the loop over the active site. Movement of the loop results in the replacement of His254 $N^{\epsilon 2}$ by Thr110 $O^{\gamma 1}$ as the hydrogen-bonding partner for O62 of CA-asp and Thr109 interacts with O5 of CA-asp to lock the conformation of the substrate (Scheme 2, state B). The carboxylate group of Asp250 that is positioned 2.7 Å from

Scheme 3: Reactions Catalyzed by DHOase and DHPase

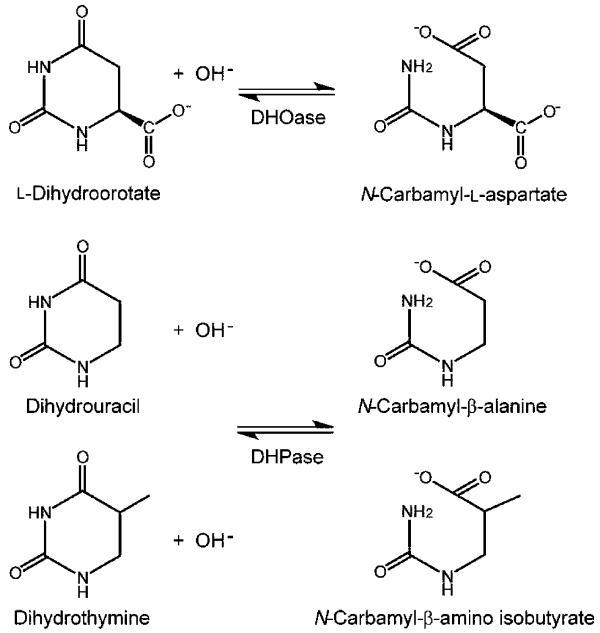

the amide nitrogen (N3) of CA-asp in the wild-type structure abstracts a proton from N3 of CA-asp to initiate the nucleophilic attack of the amide nitrogen on the carboxylate group of CA-asp (C4/O4/O5). A tetrahedral transition-state intermediate is formed and stabilized by the interaction with Thr109 and the two Zn atoms (Scheme 2, state C). The collapse of the tetrahedral intermediate commences with proton donation from the carboxylate group of Asp250 to cleave the C4−O bond. Once the carboxylate group is converted to the carbonyl group of DHO, a hydroxide ion

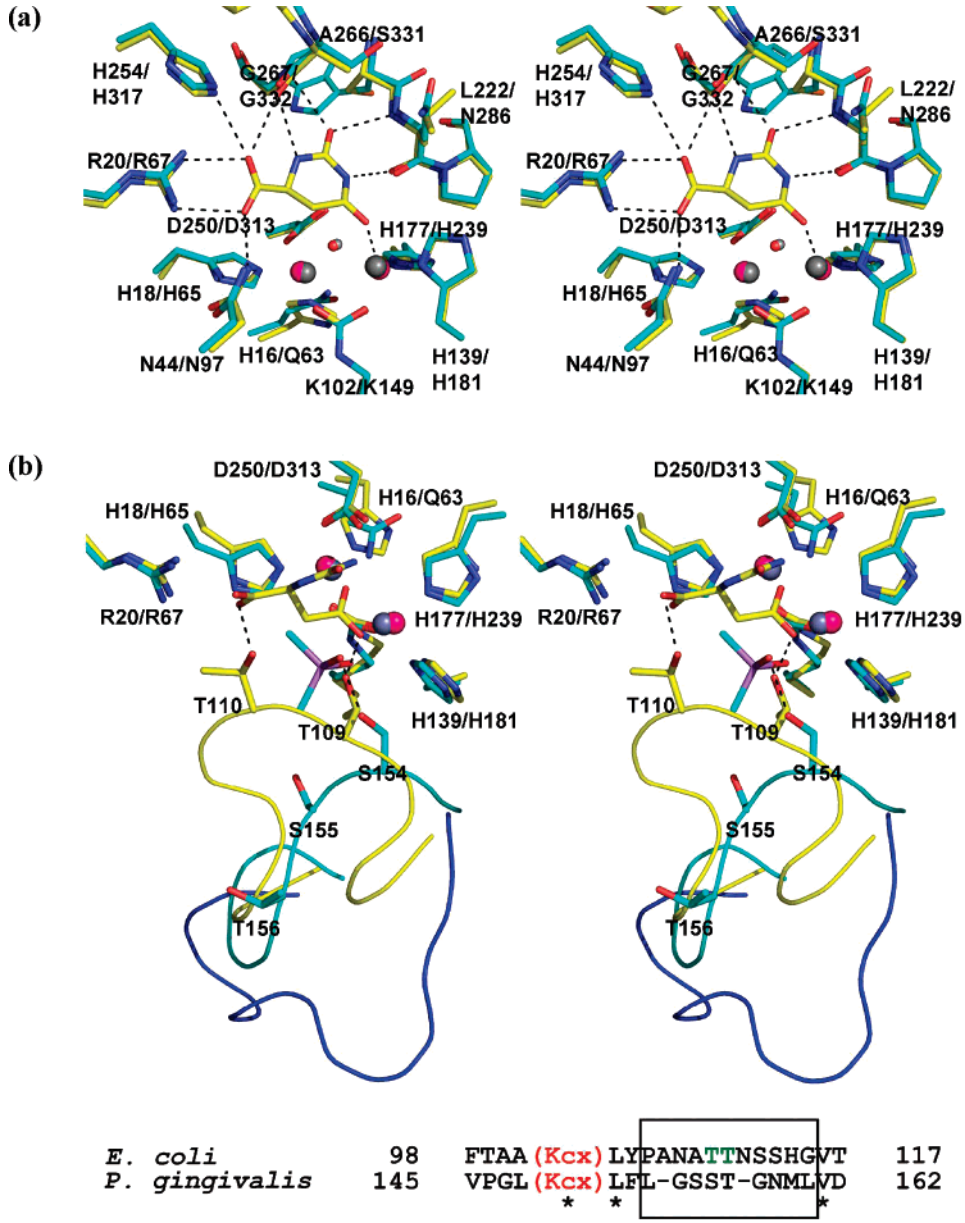

FIGURE 3: Comparison of the DHOases from *E. coli* and *P. gingivalis*. (a) Superposition of the active sites of *E. coli* DHOase with bound DHO and *P. gingivalis* DHOase (PDB code 2GWN). The C^{α} atoms of *E. coli* and *P. gingivalis* DHOases are colored in yellow and cyan, respectively. The Zn atoms and the bridging water molecule are shown as magenta and red spheres for *E. coli* DHOase and red spheres for *P. gingivalis* DHOase. Hydrogen bonds to the bound DHO in *E. coli* DHOase are depicted as dashed lines. (b) Superposition of the flexible loops. Residues 105−115 of *E. coli* DHOase and residues 152−160 of *P. gingivalis* DHOase are in ribbon presentations colored yellow (loop-in conformation of *E. coli* DHOase), blue (loop-out conformation of *E. coli* DHOase), and cyan (*P. gingivalis* DHOase). Hydrogen bonds to the bound CA-asp in *E. coli* DHOase and to the bound cacodylate ion (C, O, and As atoms colored in cyan, red, and purple, respectively) in *P. gingivalis* DHOase are indicated as dashed lines. Alignment of the residues corresponding to the flexible loops is shown below the figure. Residues corresponding to 105−115 for *E. coli* DHOase are boxed. The carboxylated lysine residues (Lys102 for *E. coli* DHOase; Lys149 for *P. gingivalis* DHOase) and two threonine residues from *E. coli* DHOase (Thr109 and Thr110) are highlighted in red and green, respectively.

bridges the two Zn atoms in a monodentate manner and the DHO molecule moves up and away from the metal sites. This causes steric pressure on residue Thr109 and release of the loop to the out conformation, concomitantly releasing the product, DHO (Scheme 2, state D). States B and D are represented by the L-CA-asp- and L-DHO-bound subunits in the structure of DHOase crystallized in the presence of L-DHO (*15*).

In the direction of DHO hydrolysis, the active form of the enzyme is proposed as one in which a hydroxide ion bridges the two Zn atoms (Scheme 2, state a). This is the state seen in the structure of ligand-free DHOase crystallized at pH 7 (*30*). Since this structure was determined at relatively high pH, it corresponds with "state a" of Scheme 2 rather than with "state A". The previously proposed terminal water molecule bound to the β-Zn atom was not observed in this structure, and we have therefore omitted it from the proposed mechanism. The nucleophilic attack at C4 of the bound DHO by the bridging hydroxide ion is facilitated by the transfer of the proton from the hydroxide ion to the carboxylate group of Asp250. Stabilization of the tetrahedral transition state is achieved via bidentate ligation to both Zn atoms and via the formation of a hydrogen bond between one of the oxygen atoms of the tetrahedral intermediate and Thr109 (Scheme

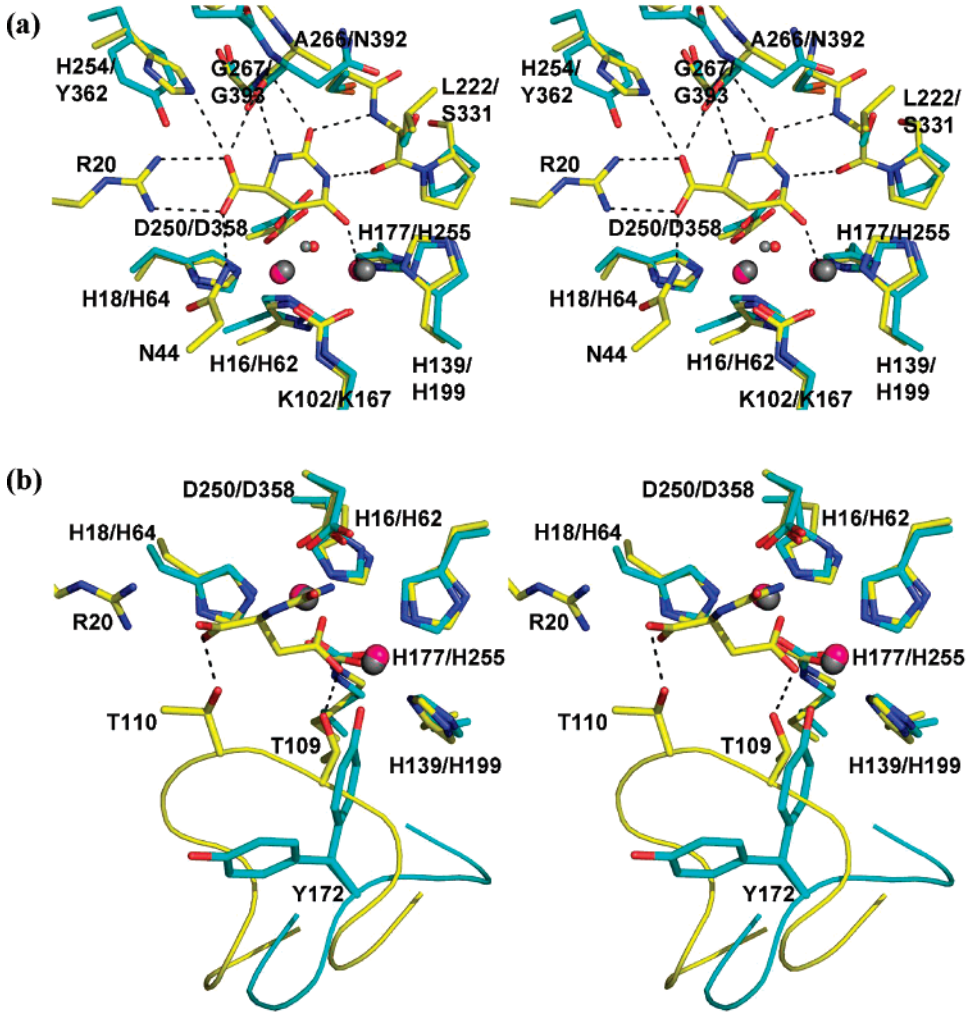

FIGURE 4: Comparison of DHOase and DHPase. (a) Superposition of the active sites of *E. coli* DHOase with bound DHO and *S. kluyveri* DHPase [PDB code 2FTY (*21*)]. The C^{α} atoms of DHOase and DHPase are colored in yellow and cyan, respectively. The Zn atoms and the bridging water molecule are shown as magenta and red spheres for DHOase and gray spheres for DHPase. Hydrogen bonds to the bound DHO in DHOase are depicted as dashed lines. (b) Superposition of residues involved in the transition-state stabilization. Residues 105−115 of DHOase and residues 170−175 of DHPase are in ribbon presentations colored yellow and cyan, respectively. Hydrogen bonds to the bound CA-asp in DHOase are indicated as dashed lines.

2, state C). Concomitant protonation of the amide nitrogen (N3) by Asp250 assists the cleavage of the N3−C4 bond, leading to collapse of the transition state and CA-asp formation (Scheme 2, state B).

According to transition-state theory, an enzyme spends the least time in the most important step of the catalytic cycle, namely, in the transition state. Reaching the transition state from the Michaelis complex requires the correct alignment of essential catalytic groups in three-dimensional space and substrate conformational changes (*47*). In *E. coli* DHOase, the movement of the flexible loop enables Thr109 and Thr110 to provide the productive binding of CA-asp and to stabilize the transition-state intermediate. Removal of water molecules from the active site cavity provided by movement of the flexible loop shields the substrate and transition-state intermediate from the bulk solvent, creating a low dielectric environment where electrostatic interactions are enhanced, thereby increasing the affinity of the enzyme for the substrate and transition-state intermediate.

Relevance of Loop Movements in DHOases. In our previous study, we suggested that the hydrogen-bonding interactions between loop residues and bound CA-asp may be important for many DHOases based on sequence homology with the *E. coli* enzyme (*15*). The flexible loop in all of the known type II DHOases is highly conserved, and the two Thr residues (Thr109 and Thr110) found in *E. coli* DHOase are invariant. The recently deposited structure of the DHOase from *P. gingivalis* provides further evidence for this hypothesis. Although originally classified as a type I DHOase on the basis of its size and amino acid sequence, the structure of the active site of *P. gingivalis* DHOase is indistinguishable from that of *E. coli* DHOase and has the characteristic binuclear Zn center (Figure 3a). The atoms involved in substrate binding superpose well within the coordinate errors of the two structures. The only major difference observed between the two active sites is the substitution of one of the Zn ligand residues: His16 in *E. coli* DHOase is replaced by Gln63 in *P. gingivalis* DHOase. *P. gingivalis* DHOase was crystallized in cacodylate buffer. The cacodylate binds in the active site, and one of its oxygen atoms forms a hydrogen bond with a Ser in the mobile loop, which adopts the loop-in conformation (Figure 3b). Stabilization of the loop-in conformation by a bound ligand is consistent with the role for the loop proposed in *E. coli*

DHOase. The loop (residues 152−160) is two residues shorter than the *E. coli* counterpart but has three consecutive residues (Ser154, Ser155, and Thr156) that could play equivalent roles to Thr109 and Thr110 of *E. coli* DHOase.

Pyrimidine Synthesis vs Degradation. As a part of the pyrimidine synthetic pathway, DHOase activity is important in providing essential pyrimidine nucleotides. In resting or fully differentiated human cells, the activity of the *de novo* pathway is, in general, low when the requirement for pyrimidines is largely satisfied by the salvage pathways. The demand for nucleic acid precursors and other cellular components associated with cell proliferation increases in rapidly proliferating cells. Consequently, the activity of the *de novo* pathway is upregulated in tumors and neoplastic cells. At the other end of pyrimidine pathway, excess or unwanted pyrimidines need to be degraded to regulate the pyrimidine pool size. This catabolic pathway involves dihydropyrimidinase (DHPase) that catalyzes the mirror reaction of DHOase, ring hydrolysis of 5,6-dihydrouracil (DHU) to *N*-carbamyl-β-alanine and of 5,6-dihydrothymine to *N*-carbamyl-β-aminoisobutyrate (Scheme 3). Both DHOase and DHPase belong to the amidohydrolase superfamily and show significant sequence similarity (*48*). The recently determined crystal structures of DHPase from *Saccharomyces kluyveri* are strikingly similar to *E. coli* DHOase both in overall structure and in the structure of its active site (*21*). The binuclear Zn centers are almost identical (Figure 4a). DHO and DHU are bound in very similar ways via hydrogen bonds involving atoms N1, O2, and N3 of the product/substrate with backbone atoms (Leu222 N and O and Ala266 O for DHOase; S331 N and O and N392 O for DHPase). However, three residues (Arg20, Asn44, and His254 for DHOase) whose side chains interact with the exocyclic carboxylate group of DHO are absent in DHPase, which may explain the substrate selectivity for DHU over DHO in DHPase. How DHOase discriminates DHO over DHU is, however, unclear. The minimal structural differences between the active sites indicate that DHU would fit in the active site of DHOase. In an attempt to probe this selectivity, the structure of DHOase crystallized in the presence of DHU was refined (unpublished data). There was no significant electron density attributable to DHU in the active site. Attempts to convert the substrate specificity of DHOase to DHPase by mutating three residues that interact with the carboxylate group of DHO were not successful (unpublished data), suggesting that subtle differences between the active sites of the two enzymes determine substrate specificity.

No flexible loop movement was observed in the structures of DHPase despite the expectation of a similar transition-state intermediate. In DHPase, a different mechanism for transition-state stabilization is proposed. The corresponding loop (residues 170−175), located between β4 and α4 of the TIM barrel in DHPase, is shorter than that (residues 105−115) in DHOase. Instead of using the flexible loop to recruit Thr109 to interact with the substrate as seen in *E. coli* DHOase, DHPase has a conserved tyrosine residue (Tyr172 in *S. kluyveri* DHPase), the side chain of which has a different orientation depending on the ligand status. Tyr172 is oriented toward the bulk solvent and away from the active site in ligand-free DHPase but toward the active site, placing its OH group close to the O4 atom of the bound DHU (*21*). Tyr172 OH in the ligand-bound DHPase superposes closely on Thr109 $O^{\gamma 1}$ of DHOase in the loop-in conformation (Figure 4b). The two enzymes sharing structural and sequence similarities presumably originated from the same ancestral gene. They have diverged into enzymes with different substrate specificities by amino acid changes, insertions, and deletions. During the course of evolution, DHOase has adopted a flexible loop movement to stabilize the transition-state intermediate, and DHPase with a shorter loop has used the movement of a side chain to achieve the same result.

SUPPORTING INFORMATION AVAILABLE

One table of mutagenic PCR primers. This material is available free of charge via the Internet at http://pubs.acs.org.

REFERENCES

1. Christopherson, R. I., and Jones, M. E. (1979) Interconversion of carbamyl-L-aspartate and L-dihydroorotate by dihydroorotase from mouse Ehrlich ascites carcinoma, *J. Biol. Chem. 254*, 12506−12512.
2. Porter, T. N., Li, Y., and Raushel, F. M. (2004) Mechanism of the dihydroorotase reaction, *Biochemistry 43*, 16285−16292.
3. Evans, D. R., and Guy, H. I. (2004) Mammalian pyrimidine biosynthesis: fresh insights into an ancient pathway, *J. Biol. Chem. 279*, 33035−33038.
4. Coleman, P. F., Suttle, D. P., and Stark, G. R. (1977) Purification from hamster cells of the multifunctional protein that initiates *de novo* synthesis of pyrimidine nucleotides, *J. Biol. Chem. 252*, 6379−6385.
5. Krungkrai, J., Cerami, A., and Henderson, G. B. (1990) Pyrimidine biosynthesis in parasitic protozoa: purification of a monofunctional dihydroorotase from *Plasmodium berghei* and *Crithidia fasciculata*, *Biochemistry 29*, 6270−6275.
6. Ahuja, A., Purcarea, C., Ebert, R., Sadecki, S., Guy, H. I., and Evans, D. R. (2004) *Aquifex aeolicus* dihydroorotase: association with aspartate transcarbamoylase switches on catalytic activity, *J. Biol. Chem. 279*, 53136−53144.
7. Robles Lopez, S. M., Hortua Triana, M. A., and Zimmermann, B. H. (2006) Cloning and preliminary characterization of the dihydroorotase from *Toxoplasma gondii*, *Mol. Biochem. Parasitol. 148*, 93−98.
8. Fields, C., Brichta, D., Shepherdson, M., Farinha, M., and O'Donovan, G. (1999) Phylogenetic analysis and classification of dihydroorotases: a complex history for a complex enzyme, *Pathways to Pyrimidines. An International Newsletter 7*, 49−63.
9. Huang, D. T., Kaplan, J., Menz, R. I., Katis, V. L., Wake, R. G., Zhao, F., Wolfenden, R., and Christopherson, R. I. (2006) Thermodynamic analysis of catalysis by the dihydroorotases from hamster and *Bacillus caldolyticus*, as compared with the uncatalyzed reaction, *Biochemistry 45*, 8275−8283.
10. Anderson, M. A., Cleland, W. W., Huang, D. T., Chan, C., Shojaei, M., and Christopherson, R. I. (2006) ^{13}C and ^{15}N isotope effects for conversion of L-dihydroorotate to *N*-carbamyl-L-aspartate using dihydroorotase from hamster and *Bacillus caldolyticus*, *Biochemistry 45*, 7132−7139.
11. Martin, P. D., Purcarea, C., Zhang, P., Vaishnav, A., Sadecki, S., Guy-Evans, H. I., Evans, D. R., and Edwards, B. F. (2005) The crystal structure of a novel, latent dihydroorotase from *Aquifex aeolicus* at 1.7Å resolution, *J. Mol. Biol. 348*, 535−547.
12. Holm, L., and Sander, C. (1997) An evolutionary treasure: unification of a broad set of amidohydrolases related to urease, *Proteins 28*, 72−82.
13. Seibert, C. M., and Raushel, F. M. (2005) Structural and catalytic diversity within the amidohydrolase superfamily, *Biochemistry 44*, 6383−6391.
14. Thoden, J. B., Phillips, G. N., Jr., Neal, T. M., Raushel, F. M., and Holden, H. M. (2001) Molecular structure of dihydroorotase: a paradigm for catalysis through the use of a binuclear metal center, *Biochemistry 40*, 6989−6997.
15. Lee, M., Chan, C. W., Guss, J. M., Christopherson, R. I., and Maher, M. J. (2005) Dihydroorotase from *Escherichia coli*: loop movement and cooperativity between subunits, *J. Mol. Biol. 348*, 523−533.

16. Benini, S., Rypniewski, W. R., Wilson, K. S., Miletti, S., Ciurli, S., and Mangani, S. (1999) A new proposal for urease mechanism based on the crystal structures of the native and inhibited enzyme from *Bacillus pasteurii*: why urea hydrolysis costs two nickels, *Structure 7*, 205−216.
17. Jabri, E., Carr, M. B., Hausinger, R. P., and Karplus, P. A. (1995) The crystal structure of urease from *Klebsiella aerogenes*, *Science 268*, 998−1004.
18. Benning, M. M., Hong, S. B., Raushel, F. M., and Holden, H. M. (2000) The binding of substrate analogs to phosphotriesterase, *J. Biol. Chem. 275*, 30556−30560.
19. Cheon, Y. H., Kim, H. S., Han, K. H., Abendroth, J., Niefind, K., Schomburg, D., Wang, J., and Kim, Y. (2002) Crystal structure of D-hydantoinase from *Bacillus stearothermophilus*: insight into the stereochemistry of enantioselectivity, *Biochemistry 41*, 9410−9417.
20. Abendroth, J., Niefind, K., May, O., Siemann, M., Syldatk, C., and Schomburg, D. (2002) The structure of L-hydantoinase from *Arthobacter aurescens* leads to an understanding of dihydropyrimidinase substrate and enantio specificity, *Biochemistry 41*, 8589−8597.
21. Lohkamp, B., Andersen, B., Piskur, J., and Dobritzsch, D. (2006) The crystal structures of dihydropyrimidinases reaffirm the close relationship between cyclic amidohydrolases and explain their substrate specificity, *J. Biol. Chem. 281*, 13762−13776.
22. Washabaugh, M. W., and Collins, K. D. (1984) Dihydroorotase from *Escherichia coli*. Purification and characterization, *J. Biol. Chem. 259*, 3293−3298.
23. Washabaugh, M. W., and Collins, K. D. (1986) Dihydroorotase from *Escherichia coli*. Sulfhydryl group-metal ion interactions, *J. Biol. Chem. 261*, 5920−5929.
24. Brown, D. C., and Collins, K. D. (1991) Dihydroorotase from *Escherichia coli*. Substitution of Co(II) for the active site Zn(II), *J. Biol. Chem. 266*, 1597−1604.
25. Kelly, R. E., Mally, M. I., and Evans, D. R. (1986) The dihydroorotase domain of the multifunctional protein CAD. Subunit structure, zinc content, and kinetics, *J. Biol. Chem. 261*, 6073−6083.
26. Williams, N. K., Peide, Y., Seymour, K. K., Ralston, G. B., and Christopherson, R. I. (1993) Expression of catalytically active hamster dihydroorotase domain in *Escherichia coli*: purification and characterization, *Protein Eng. 6*, 333−340.
27. Huang, D. T., Thomas, M. A., and Christopherson, R. I. (1999) Divalent metal derivatives of the hamster dihydroorotase domain, *Biochemistry 38*, 9964−9970.
28. Williams, N. K., Manthey, M. K., Hambley, T. W., O'Donoghue, S. I., Keegan, M., Chapman, B. E., and Christopherson, R. I. (1995) Catalysis by hamster dihydroorotase: zinc binding, site-directed mutagenesis, and interaction with inhibitors, *Biochemistry 34*, 11344−11352.
29. Zimmermann, B. H., Kemling, N. M., and Evans, D. R. (1995) Function of conserved histidine residues in mammalian dihydroorotase, *Biochemistry 34*, 7038−7046.
30. Lee, M., Chan, C. W., Graham, S. G., Christopherson, R. I., Guss, J. M., and Maher, M. J. (2007) Structures of ligand-free and inhibitor complexes of dihydroorotase from *Escherichia coli*: Implications for loop movement in inhibitor design, *J. Mol. Biol. 370*, 812−825.
31. Sander, E. G., Wright, L. D., and McCormick, D. B. (1965) Evidence for function of a metal ion in the activity of dihydroorotase from *Zymobacterium oroticum*, *J. Biol. Chem. 240*, 3628−3630.
32. Otwinowski, Z., and Minor, W. (1997) Processing of X-ray diffraction data collected in oscillation mode, *Methods Enzymol. 276*, 307−326.
33. Matthews, B. W. (1968) Solvent content of protein crystals, *J. Mol. Biol. 33*, 491−497.
34. Murshudov, G. N., Vagin, A. A., and Dodson, E. J. (1997) Refinement of macromolecular structures by the maximum-likelihood method, *Acta Crystallogr., Sect. D: Biol. Crystallogr. 53*, 240−255.
35. Winn, M. D., Isupov, M. N., and Murshudov, G. N. (2001) Use of TLS parameters to model anisotropic displacements in macromolecular refinement, *Acta Crystallogr., Sect. D: Biol. Crystallogr. 57*, 122−133.
36. Emsley, P., and Cowtan, K. (2004) Coot: model-building tools for molecular graphics, *Acta Crystallogr., Sect. D: Biol. Crystallogr. 60*, 2126−2132.
37. Perrakis, A., Harkiolaki, M., Wilson, K. S., and Lamzin, V. S. (2001) ARP/wARP and molecular replacement, *Acta Crystallogr., Sect. D: Biol. Crystallogr. 57*, 1445−1450.
38. Storoni, L. C., McCoy, A. J., and Read, R. J. (2004) Likelihood-enhanced fast rotation functions, *Acta Crystallogr., Sect. D: Biol. Crystallogr. 60*, 432−438.
39. Collaborative Computational Project, No. 4 (1994) The CCP4 Suite: Programs for Protein Crystallography, *Acta Crystallogr., Sect. D: Biol. Crystallogr. 50*.
40. Hooft, R. W. W., Vriend, G., Sander, C., and Abola, E. E. (1996) Errors in protein structures, *Nature 381*, 272.
41. Lovell, S. C., Davis, I. W., Arendall, W. B., III, de Bakker, P. I., Word, J. M., Prisant, M. G., Richardson, J. S., and Richardson, D. C. (2003) Structure validation by Calpha geometry: phi, psi and Cbeta deviation, *Proteins 50*, 437−450.
42. Lee, M., Maher, M. J., and Guss, J. M. (2007) Structure of the T109S mutant of *Esherichia coli* dihydroorotase complexed with the inhibitor 5-fluoroorotate: catalytic activity is reflected by the crystal form, *Acta Crystallogr., Sect. D: Biol. Crystallogr. 63*, 154−161.
43. Kempner, E. S. (1993) Movable lobes and flexible loops in proteins. Structural deformations that control biochemical activity, *FEBS Lett. 326*, 4−10.
44. Hammes, G. G. (2002) Multiple conformational changes in enzyme catalysis, *Biochemistry 41*, 8221−8228.
45. Gutteridge, A., and Thornton, J. (2004) Conformational change in substrate binding, catalysis and product release: an open and shut case?, *FEBS Lett. 567*, 67−73.
46. Gutteridge, A., and Thornton, J. (2005) Conformational changes observed in enzyme crystal structures upon substrate binding, *J. Mol. Biol. 346*, 21−28.
47. Schramm, V. L. (1998) Enzymatic transition states and transition state analog design, *Annu. Rev. Biochem. 67*, 693−720.
48. Gojkovic, Z., Rislund, L., Andersen, B., Sandrini, M. P., Cook, P. F., Schnackerz, K. D., and Piskur, J. (2003) Dihydropyrimidine amidohydrolases and dihydroorotases share the same origin and several enzymatic properties, *Nucleic Acids Res. 31*, 1683−1692.
49. DeLano, W. L. (2002) The PyMOL molecular graphics system, DeLano Scientific, San Carlos, CA.
50. Cruickshank, D. W. (1999) Remarks about protein structure precision, *Acta Crystallogr., Sect. D: Biol. Crystallogr. 55*, 583−601.

BI701098E